Pure & Appl. Chem., Vol. 64, No. 11, pp. 1629–1634, 1992.
Printed in Great Britain.

Assembly of Xe atoms in a NaA alpha cage: A Monte Carlo simulation

Paul R. Van Tassel, Claude Hall, H. Ted Davis, and Alon V. McCormick

Department of Chemical Engineering and Materials Science, University of Minnesota, Minneapolis, MN, 55455, USA

Abstract - The canonical ensemble Monte Carlo method is used to study the adsorption of Xe atoms inside of a zeolite alpha cage. The cage is modeled in 2 ways: 1) as atoms placed on the vertices and line segments of a polyhedron and, and 2) as atoms placed in their crystallographically determined positions. Discrete adsorption sites are found and they change position in response to changes in loading, cage cation content, and cage model. Thermodynamic data determined from the crystallographic model cage is in good agreement with experiment, while data obtained from the polyhedral model is only qualitatively correct. In this way we show that, in order to model adsorption in zeolites accurately, it is important to account for the precise architecture of the pore.

INTRODUCTION

Zeolites are crystalline aluminosilicates possessing a regular network of interconnected pores with molecular dimensions, a characteristic that makes them useful in catalysis, separations, and ion exchange. A detailed understanding of the adsorbed phase is crucial to the analysis of these processes. Recent advances have been accomplished through molecular computer simulation (ref. 1-6). Here we present results of Monte Carlo simulations of Xe atoms adsorbed in the alpha cage of zeolite NaA (ref. 7,8) modeled with varying degrees of accuracy.

MONTE CARLO SIMULATIONS

The canonical ensemble Monte Carlo algorithm of Metropolis (ref. 9) is performed on a system consisting of a single alpha cage containing N Xe atoms at a temperature of 300 K to generate an adsorbate distribution of minimum free energy. The length of a simulation varies from 90,000 to 200,000 steps, which follow 10,000 to 150,000 discarded steps. All computations were performed on either the Cray-2 or Cray-XMP supercomputers, made available to us by the Minnesota Supercomputer Center.

The potential energy of the Xe atoms is calculated atomistically (ref. 10) as

$$\Phi = \Phi_R + \Phi_D + \Phi_P + \Phi_{Xe\text{-}Xe} \qquad (1)$$

where the total potential energy Φ includes terms representing Xe-zeolite repulsion, Xe-zeolite attraction via induced dipole-induced dipole dispersion, Xe-zeolite attraction due to the presence of the static electric field (polarization), and Xe-Xe interactions using the Lennard-Jones potential. Potential parameters were chosen from the literature (ref. 11).

RESULTS

Due to the somewhat spherical shape of the alpha cage and other types of zeolite cages, an attempt has been made to model a zeolite cage as a sphere (ref. 2). In order to incorporate the atomic nature of a real zeolite cage into a simulation model, we, along with other researchers (ref. 1, 3-8), have modeled zeolite pores atomistically. We will discuss results based on cage models in which framework atoms are placed, in one case, on a polyhedron (with the same symmetry as the zeolite crystal structure) and, in another case, according to the known crystal structure. In this way we determine the effects (on the adsorbed phase) of the detailed atomic structure of the zeolite, where these effects are not simply due to any changes in crystalline symmetry or size of the quasi-sperical cavity.

Truncated cuboctahedral model alpha cage

The NaA alpha cage (Fig. 1) possesses the symmetry of a truncated cuboctahedron in which the vertices represent either silicon or aluminum atoms. These are connected by bridging oxygen atoms, which protrude slightly inward toward the cage center. As a first approximation, we model the alpha cage as a truncated cuboctahedron with oxygen atoms located at the centers of the line segments. To compensate for this oxygen placement, we employ a somewhat smaller cage diameter by imposing a spacing between nearest neighbor vertices equal to the O-O distance of an isolated SiO_4 tetrahedron (2.6 Å) (ref. 12).

Sodium cations are located in the centers of the 6- and 8-membered rings for a cation-rich alpha cage, and only the 6-membered rings in the cation-poor cage. The negative charge required to offset the cation charge is spread equally over the oxygen atoms. The cation-rich cage closely approximates true NaA, while the cation-poor cage represents the effect of dealumination.

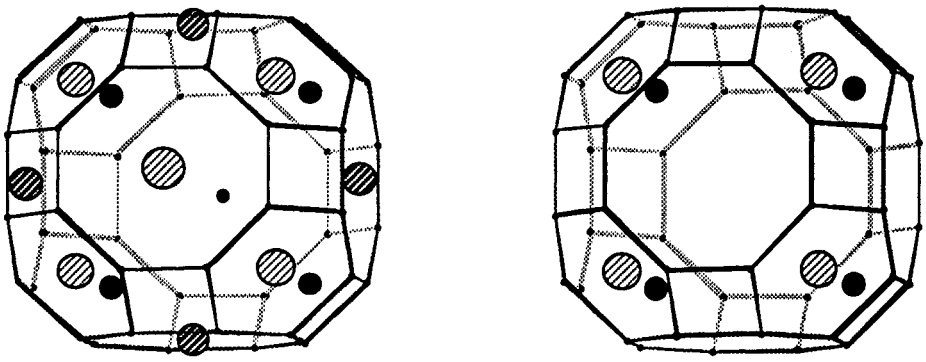

Fig. 1. The Cation-rich (left) and cation-poor (right) alpha cages represented as truncated cuboctahedra. Vertices represent either silicon or aluminum atoms. Circles represent sodium cations, which are shaded and decreasing in size to provide front to back perspective.

The average potential energy of the adsorbed Xe is calculated as a function of loading (Fig. 2-a). The cation-rich cage adsorbs 4 atoms favorably, while the addition of a fifth Xe atom causes an energy increase. When Na cations are removed from the 8-membered rings (cation-poor cage), the capacity is increased to 6 Xe atoms. The less polar, cation-poor cage not only has a higher capacity for Xe adsorption, it also adsorbs Xe with greater energetic strength. The isosteric heat of adsorption may be estimated for the low loading regime (ref. 13) by

$$-q_{iso} = \langle\Phi\rangle_1 - kT \qquad (2)$$

where $\langle\Phi\rangle_1$ is the average potential energy of 1 Xe atom. The isosteric heats of adsorption are 35.4 and 38.9 kJ/mol, for the cation rich and cation-poor cages respectively. The experimental value for zeolite CaA (a close structural analog to NaA) at T=423 K is 20.9 kJ/mol (ref. 14). The discrepancy between simulation and experiment is mainly due to inexact framework oxygen placement and will be discussed below.

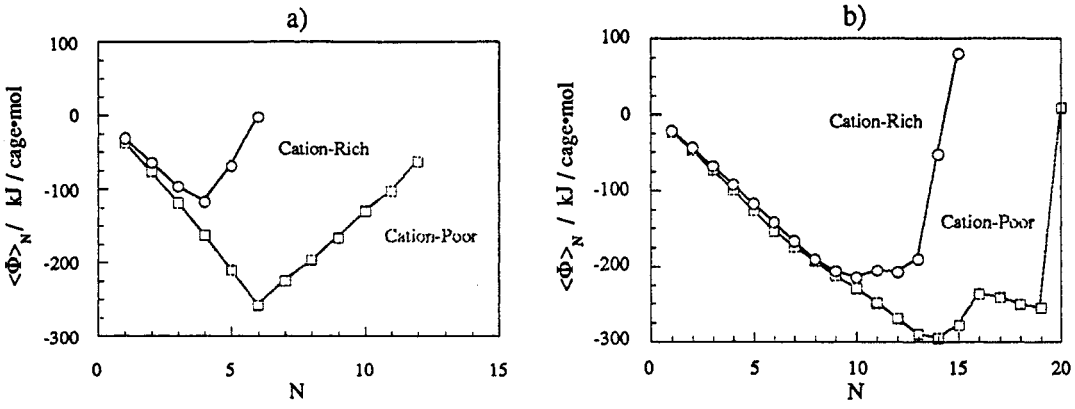

Fig. 2. The average potential energy versus cage loading in a) the polyhedral model cage and b) the crystallographic model cage.

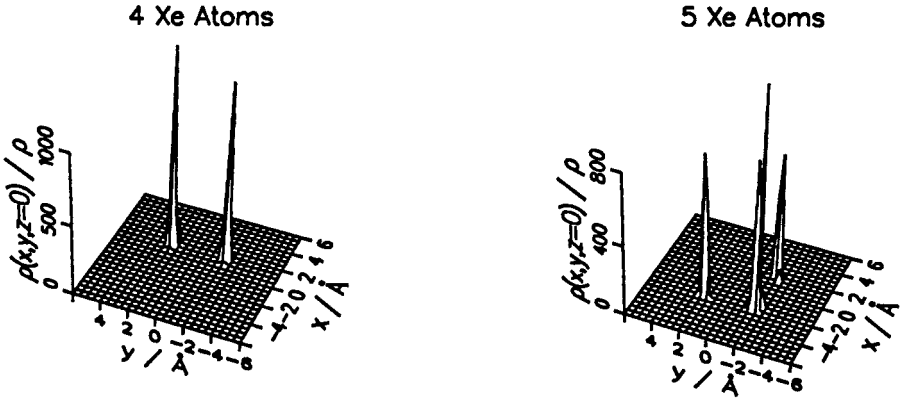

Fig. 3. The density distribution function for the cation-rich polyhedral cage at loadings of 4 and 5 Xe atoms. The lines x=0 and y=0 in the z=0 plane connect the centers of the 8-membered ring (Fig. 1).

The positions of the adsorption sites may be determined by viewing the density distribution function along a plane bisecting the alpha cage. The density distribution in the cation-rich cage (Fig. 3) appears as peaks in front of the 4-membered ring (figure 1) of the cage structure. There are 12 such rings, and the connection of their nearest neighbors forms a cuboctahedron (Fig. 4). The density distribution of Xe in the cation-poor cage (Fig. 5) appears as 4 peaks, each facing a vacant 8-membered ring. The connection of the nearest neighbors of these 6 rings forms an octahedron (Fig. 4). Note that at a loading of 7 Xe, this symmetry is broken somewhat by a Xe atom adsorbed near an 8-membered window. Thus, we see how a changes in the cation arrangement or the sorbate loading may induce a change in the symmetry of the adsorbed phase.

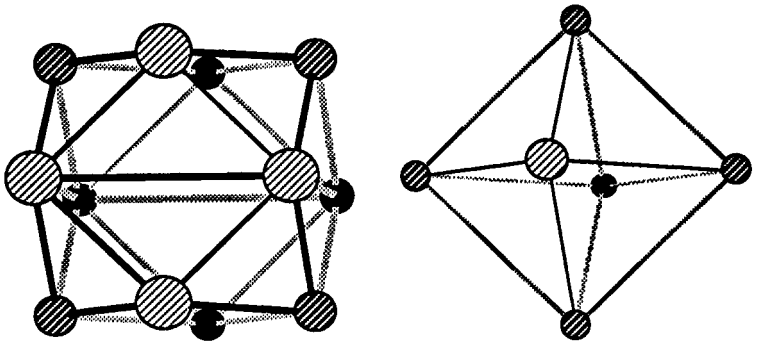

Fig. 4. The cuboctahedron (left) and octahedron (right). These polyhedrons represent the adsorbed phase symmetries found in the cation-rich and cation-poor alpha cages, respectively, for both the polyhedral and crystallographic cage models.

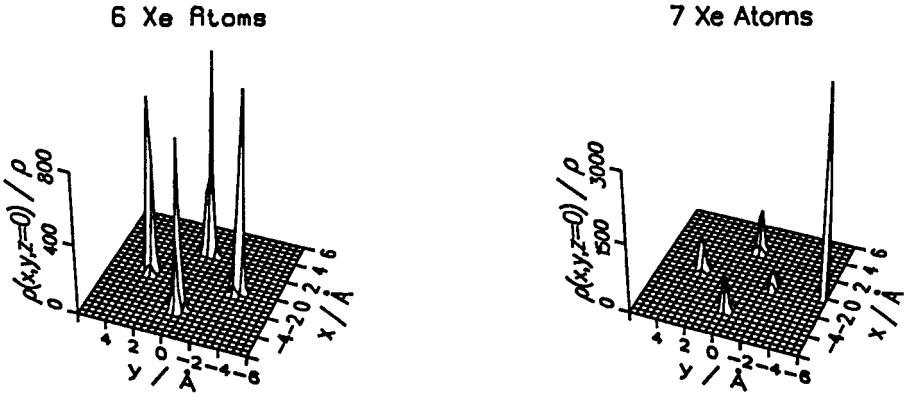

Fig. 5. The density distribution function for the cation-poor polyhedral cage at loadings of 6 and 7 Xe atoms.

Crystallographic cage model

For a more realistic description, we also model the alpha cage as an assembly of atoms positioned according to crystallographic data (ref. 15). We again consider the Na cations in the 6- and 8-membered rings to be located in the ring centers (the latter being a slight deviation from the crystallographic position).

The average potential energy as a function of cage loading is shown in Fig. 2-b. The cage capacity and the magnitude of the average potential energy are larger in the cation-poor cage, the same trend exhibited by the polyhedral model. However, the capacity of the crystallographic cage is much greater than that of the polyhedral cage. The isosteric heat determined by (2) is 25.3 and 26.7 kJ/mol for the cation-rich and cation-poor cages, respectively. These compare much more favorably with the experimental value (CaA, 423 K) of 20.9 kJ/mol.

The density distribution functions for both cation contents (Fig. 6 and 7) reveal similar arrangements as those observed in the polyhedral cage, but their are significant differences. First, whereas only some of the possible sites were occupied during the course of the simulation in the polyhedral cage, all possible sites are occupied in the crystallographic cage. Second, a loading of 7 Xe no longer breaks the octahedral symmetry. Finally, we see that at higher loadings, additional peaks form away from the original sites. An additional site is located at the cation-rich cage center and is occupied when the cage loading reaches 13 Xe. Additional sites are also found in the cation-poor cage at cuboctahedral positions and are occupied when loadings approach 14 Xe atoms.

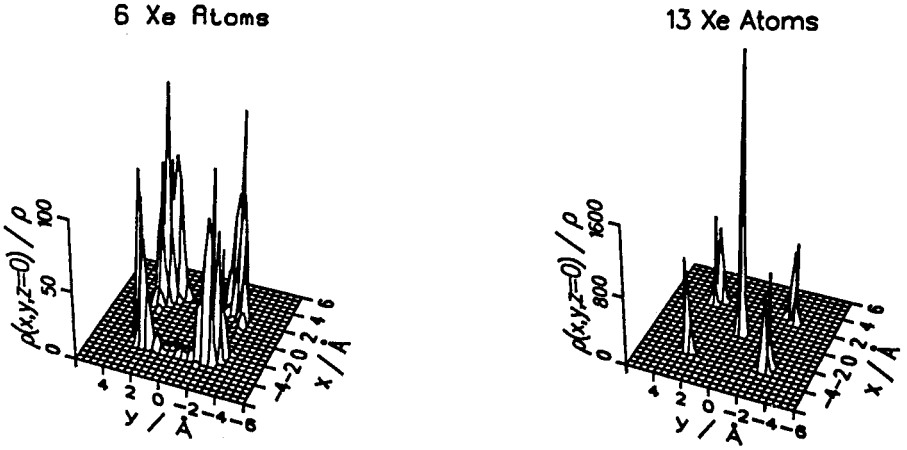

Fig. 6. The density distribution function for the cation-rich crystallographic cage at loadings of 6 and 13 Xe atoms.

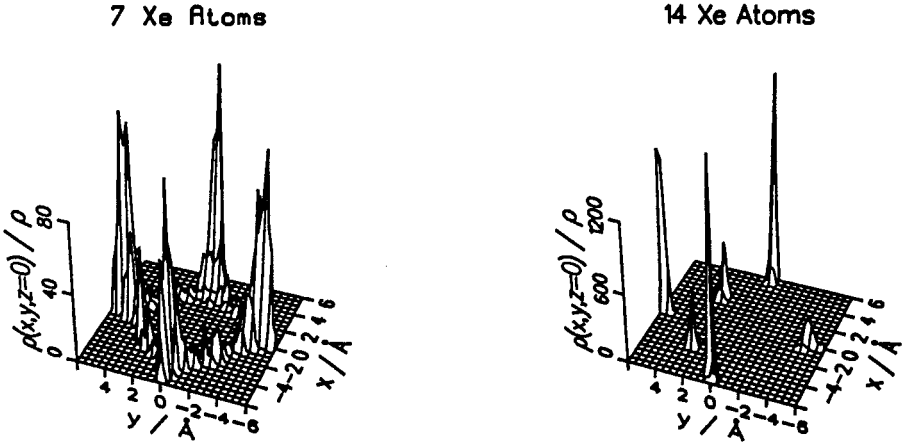

Fig. 7. The density distribution function for the cation-poor crystallographic cage at loadings of 7 and 14 Xe atoms.

DISCUSSION

The symmetry associated with the adsorbed phase strongly depends on the number and positions of the cations, but is independent of whether we model the cages as a polyhedron or as atoms in crystallographically correct positions. When the 8-membered rings are vacant (cation-poor cage), Xe density maxima are established in front of these rings, and these six positions possess octahedral symmetry. The addition of cations to the 8-membered rings shifts the density maxima to twelve sites facing the 4-oxygen ring. These 12 sites have cuboctahedral symmetry.

The cation-poor cage, though less polar, possesses a greater adsorption capacity and adsorbs Xe more energetically than the cation-rich cage. The removal of cations has increased the volume available to adsorbed Xe and has caused the most favored adsorption sites to change. These new sites are more favorable than those present in the cation-rich cage. Thus, steric effects of framework cations play a larger role in adsorption than charge effects.

Though the polyhedral cage model predicts an adsorbed phase symmetry in qualitative agreement with predictions of the crystallographic cage model, large quantitative differences exist. First, the isosteric heat of adsorption is about 70% greater in the polyhedral cage. Also, the polyhedral cage capacity is much smaller than that of the crystallographic cage (4 Xe vs. 10 for cation-rich, 6 Xe vs. 14 for cation-poor). The experimental heat of adsorption is much closer to that found in the crystallographic cage model. Also, it is possible to experimentally isolate (cation-rich) alpha cages with occupancies of 7 Xe in NaA (ref. 16-18). This loading would seem very unlikely given the cage capacity for the polyhedral model, but is more plausible given the capacity of the crystallographically modeled cage.

The additional capacity in the crystallographic model is due in part to the ability of the cage to allow for additional adsorption sites to form following saturation of the primary sites. The cation-rich-cage may accommodate a 13th Xe at the cage center, while the cation-poor cage may form cuboctahdral sites. These additional sites are energetically disfavored in the polyhedral cage.

Though each adsorption site in the crystallographic cages (Fig. 5 and 6) is sampled over the course of the simulation at all loadings, this is not the case in the polyhedral cages. Some cuboctahedral peaks are absent in the cation-rich cage density profile (Fig. 3). Also, the 7th Xe in the polyhedral cation-poor cage (Fig. 7) adsorbs near one of the six possible vacant 8-membered rings and remains there for the entire simulation. This inefficient site sampling may imply that energetically deeper potential wells exist in the polyhedral cages. It may also reflect the differences in site-site proximity of the two models (the occupancy of a site may kinetically hinder the movement of a Xe atom to an adjacent site). In either case, a less mobile adsorbed phase is predicted by the polyhedral model.

The lower cage capacity and higher adsorption energy observed in the polyhedral cage may be explained by the fact that this model cage must be reduced in size somewhat to compensate for the inexact oxygen positions. The polyhedral cage size is based on a nearest-neighbor vertex distance equal to the O-O distance in an isolated SiO_4 tetrahedron. Although this method of determining cage size is quite general, it is also quite arbitrary. Neglecting this concern, we see that the slight framework modifications made when going to the crystallographic model cause significant differences in the adsorption energy, cage capacity, and, to a lesser degree, adsorption site location.

CONCLUSIONS

Using the Monte Carlo method to calculate equilibrium Xe atom distributions in the alpha cage of zeolite NaA modeled 1) as a polyhedron and 2) according to crystallographic data, it is clear that the symmetry of the primary adsorption sites is dictated by the cage cation content, while the isosteric heat and capacity for adsorption depend also on the nature of the cage model. We conclude that slight structural changes in the zeolite framework may cause large changes in adsorbate configurations and energetics. Thus, it is important to use the most accurate crystallographic model available in trying to simulate the distribution of adsorbates in zeolites.

Acknowledgements

P. Van Tassel was supported by grants from the ACS Petrolium Research Fund and from NSF. C. Hall was supported by an undergraduate research supplement from NSF.

REFERENCE

1. G. B. Woods and J. S. Rowlinson, J. Chem. Soc., Faraday Trans. 2 85, 765-781 (1989).
2. G. B. Woods, A. Z. Panagiotopoulos, and J. S. Rowlinson, Molecular Physics 63, 49-63 (1988).
3. J. L. Soto and A. L. Myers, Molecular Physics 42, 971-983 (1982).
4. H. Kono and A. Takasaka, J. Phys. Chem. 91, 4044-4055 (1987).
5. D. M. Razmus and C. K. Hall, AIChE Journal 37, 769-779 (1991).
6. R. Q. Snurr, R. L. June, A. T. Bell, and D. N. Theodorou, Molecular Simulation, in press.
7. P. R. Van Tassel, H. T. Davis, and A. V. McCormick, Molecular Physics 73, 1107-1125 (1991).
8. P. R. Van Tassel, H. T. Davis, and A. V. McCormick, submitted to Molecular Physics.
9. N. Metropolis, A. W. Rosenbluth, M. N. Rosenbluth, A. H. Teller, and E. Teller, J. Chem. Phys. 21, 1087-1092 (1953).
10. A. G. Bezus, A. V. Kiselev, A. A. Lopatkin, and P. Q. Du, J. Chem. Soc., Farad. Trans. 2 74, 367-379 (1977).
11. A. V. Kiselev and P. Q. Du, Dokl. Akad. Nauk SSSR 238, 384-397; 241, 386-401 (1978).
12. D. W. Breck, Zeolite Molecular Sieves, p. 50, Wiley-Interscience, New York (1974).
13. D. M. Ruthven, Principles of Adsorption and Adsorption Processes, p. 34, Wiley-Interscience, New York (1984).
14. R. M. Barrer, R. Papadopoulos, and J. D. Ramsay, Proc. R. Soc. Lond. A. 326, 331-345 (1972).
15. R. Y. Yanagida, A. A. Amaro, and K. Seff, J. Phys. Chem. 77, 805-809 (1973).
16. A. V. McCormick and B. F. Chmelka, Molecular Physics 73, 603-622 (1991).
17. M. G. Samant, L. C. de Menorval, R. A Dalla-Betta, and M. Boudart, J. Phys. Chem. 92, 3937-3942 (1988).
18. S. S. Nivarthi and A. V. McCormick, submitted to J. Phys. Chem.